Journal of
Composites Science

MDPI

Article

A Study on the Structural Features of Amorphous Nanoparticles of Ni by Molecular Dynamics Simulation

Tuan Tran Quoc [1], Dung Nguyen Trong [2,3,*], Van Cao Long [2], Umut Saraç [4] and Ştefan Ţălu [5]

[1] Faculty of Basic Science, University of Transport Technology, 54 Trieu Khuc, Thanh Xuan, Hanoi 100000, Vietnam
[2] Institute of Physics, University of Zielona Góra, Prof. Szafrana 4a, 65-516 Zielona Góra, Poland
[3] Faculty of Physics, Hanoi National University of Education, 136 Xuan Thuy, Cau Giay, Hanoi 100000, Vietnam
[4] Department of Science Education, Bartın University, Bartın 74100, Turkey
[5] The Directorate of Research, Development and Innovation Management (DMCDI), Technical University of Cluj-Napoca, 15 Constantin Daicoviciu Street, 400020 Cluj-Napoca, Romania
* Correspondence: dungntdt2018@gmail.com

Abstract: This study deals with the impact of the heating rate (HR), temperature (T), and the number of atoms (N) on the structural features of amorphous nanoparticles (ANPs) of Ni by molecular dynamics simulation (MDS) with the Pak–Doyama pair interaction potential field (PD). The obtained results showed that the structural features of ANPs of Ni are significantly affected by the studied factors. The correlation between the size (D) and the N was determined to be $D \sim N^{-1/3}$. The energy (E) was proportional to N^{-1}, and the Ni-Ni link length was 2.55 Å. The glass transition temperature (T_g) derived from the E-T graph was estimated to be 630 K. An increase in the HR induced a change in the shape of the ANPs of Ni. Furthermore, raising the HR caused an enhancement in the D and a decrement in the density of atoms. The obtained results are expected to contribute to future empirical studies.

Keywords: amorphous Ni nanoparticles; number of atoms; glass temperature; heating rate; molecular dynamics; structural properties

Citation: Tran Quoc, T.; Nguyen Trong, D.; Cao Long, V.; Saraç, U.; Ţălu, Ş. A Study on the Structural Features of Amorphous Nanoparticles of Ni by Molecular Dynamics Simulation. *J. Compos. Sci.* **2022**, *6*, 278. https://doi.org/10.3390/jcs6090278

Academic Editor: Stelios K. Georgantzinos

Received: 14 August 2022
Accepted: 16 September 2022
Published: 19 September 2022

1. Introduction

Nanoparticles (NPs) are very small particles ranging in size from 1 nm to 100 nm [1–4]. They exhibit unique and novel chemical and physical properties compared to their bulk materials [4–7]. Therefore, researchers have focused on new studies to decrease the size of bulk materials to the nanoscale. For this purpose, many theoretical (mean-field theory, etc.), experimental (electrodeposition, etc.), and simulation (molecular dynamics (MD), etc.) methods have been developed to fabricate NPs and nanomaterials and investigate their characteristic properties in detail [2,8–11]. In particular, the simulation methods have enabled the detailed analysis of the microstructure of ANPs at the atomistic level [12]. Among the simulation methods, MD is widely used to examine the crystallization process of Ni NPs [13]. In the studies, the nucleation and evolution of defects in Fe NPs [14], the separation of Fe crystal from amorphous FeB NPs [15], the local structure of the liquid and amorphous states of Al materials [16], and the effect of amorphous surface layers on the deformation process and mechanical features of Ni NPs [6] have been studied by means of the MDS method. In recent years, ANPs have received great attention for science and technology because of their exceptional properties [6,12,17]. Among them, Ni ANPs have found important applications in a wide variety of scientific and technological areas and functional devices [4,13,17–24].

Therefore, many studies have been focused on the structure of ANPs of Ni materials [25,26]. A study investigated the size (D) dependence of the Curie phase transition temperature (T_c) in Ni NPs using a theoretical model [27]. It was found that increasing the D of the Ni NPs from 24 to 200 nm leads to a gradual enhancement in the T_c from 593 K to 627 K [27]. Studies showed that T_c of Ni NPs is lower than that of bulk Ni (631 K) [27,28],

and a nonmetal–metal transition occurs with the increase in the density of Ni atoms [29], revealing a strong size effect. Ni NPs exhibit a large crystalline capacity and a high melting point, which enables them to be used as glucose-detecting electrodes [30]. In the studies, the shape and size of the NPs have been tuned using heterogeneous catalysts [31–34]. The studies showed that NPs can be obtained in sizes smaller than 3 nm [35,36] and 2 nm [37]. The melting temperature (T_m) of amorphous Ni material is 1728 K [26]. It was reported that Ni nanowires exhibit a much lower T_m compared to the T_m of bulk Ni [38]. In some studies, the correlation between the D and the number of atoms (N) was found to be $D \sim N^{-1/3}$ [39,40]. The studies also showed that D is proportional to $N^{-1/3}$ [38,41–47], and the T_m is proportional to $N^{-1/3}$ and D^{-1} [38,41,42,45–47].

It was found that increasing N from 336 to 8007 caused an enhancement in the T_m of the Ni nanoclusters from 980 to 1380 K [41]. It was shown that the T_m is affected not only by the size of the metal nanocrystals but also by their shape and dimension [48]. The glass transition temperature (T_g) for a bulk material is believed to be less than 1/2 T_m, and thus for bulk Ni material it is expected to be around 600 K [41]. The T_g was determined to be 800 K for glassy Ni with N = 4000 atoms using the MDS method [45]. Studies on the structural features of Ni NPs indicated that the closest interconnection distances of bulk Ni, crystallized Ni NPs, and Ni ANPs are 2.43 Å [49], 2.45 Å [40], and 2.52 Å [50], respectively. Considering the structural properties of Ni NPs summarized above and our recent published works on Fe [37,51], Al [52,53], Ag [54], Cu [55], Ni [17,40], and the mechanical properties of Ni nanomaterials [56], the effects of factors on the structural features of Ni ANPs have continued to be examined using the MDS method [57,58]. Based on the previously obtained results, amorphous Ni nanoparticles [40] have been successfully studied by scientists in correlation with the number of atoms, temperature, annealing time on the structure, crystallization process, and crystallization temperature. In addition, in a new study, scientists also examined new influencing factors (such as the heating rate, number of atoms, and temperature) on the characteristics of the structure of amorphous Ni nanoparticles [17,40,50]. The obtained results show that when increasing the heating rate the nanoparticles are broken at the heating rate of 10^8 K/s, which leads to an increase in the size (D) with small values. The E also decreases with small values and increases suddenly at a heating rate of 10^8 K/s. Furthermore, when increasing the number of atoms leads to D increasing, E decreases; when there is an increase in the temperature (T), D and r have constant values, E increases, and the glass temperature (T_g) has a value of T_g = 630 K. The obtained results will be the basis for experimental studies on amorphous Ni nanoparticles in the future, with aims to create useful materials for application in life.

2. Method of Calculation

Initially, to model the Ni NPs, the atoms were randomly seeded into a sphere. Then, it was placed the model in the Pak–Doyama pair interaction potential field (PD) with the free boundary condition [15,50,59], in accordance with Equation (1):

$$U(r) = A(r + B)^4 + C(r + D)^2 + E \quad (1)$$

where, U(r) represents the interaction potential, r is the distance between atoms, and A, B, C, D, and E are the constants of Ni NPs. The values applied in the model are given in Table 1.

Table 1. The values of model for the Ni NPs.

Values	Ni	Values	Ni
A	−0.12929	**D**	−2.50849
B	−1.82709	**E**	−0.135705
C	1.16473		

The D values of the NPs were estimated using Equation (2):

$$\rho = \frac{N}{V} \rightarrow D = 2\left(\frac{3N}{4\pi\rho}\right)^{\frac{1}{3}} \quad (2)$$

where, N is the number of NPs and ρ is the density, with ρ = 7.81 g·cm^{-3}.

First, the ANPs of Ni_{2048}, Ni_{2916}, Ni_{4000}, Ni_{5324}, Ni_{6912}, Ni_{8788} at T = 300 K with a 10^6 K/s heating rate (HR) were formed. In addition, the time simulation for each simulation step of MDS was 0.46 fs. Then, the HR was increased from 5 × 10^5 to 10^8 K/s with the nanoparticle Ni_{5324} at temperature (T), T = 300 K, and T was raised from 300 to 1100 K with Ni_{5324} at a constant HR of 10^6 K/s.

The structural features were examined by the MDS method with the embedded Pak–Doyama potential, which was combined with the Verlet algorithm and the average coordination number (CN), $CN = 4\pi\rho\int_0^{r_1} g(r)r^2dr$.

During the simulation, it was applied the heating process based on the laws by Nosé [60], the equation by Hoover [61], and the defined radial distribution function (RDF) [62–65].

The first peak height of the RDF is $g(r) = \frac{n(r)}{4\pi r^2 dr\rho_0}$, and r shows the first position of the RDF. The n and ρ_0 represent the number of atoms and the atomic density, respectively.

The T_g was determined from the correlation between the E and the T. The centrosymmetric parameter [46,66], the bond angle method [67], the bond order method [68], and the approach method for amorphous materials [69] were used to check the accuracy of the obtained data.

3. Results and Discussions

3.1. Structural Characteristic Quantities

To study the specific quantities for the structure of the Ni ANPs, we chose Ni_{5324} ANPs with a heating rate of 10^6 K/s at T = 300 K. The obtained results are shown in Figure 1.

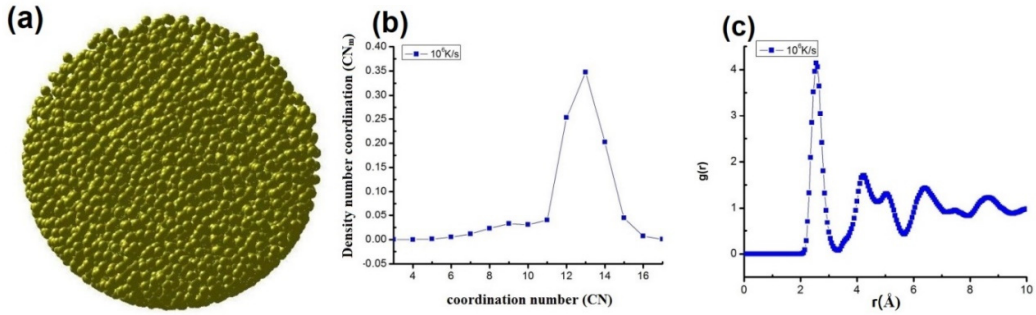

Figure 1. The shape (**a**), CNs (**b**), and RDF (**c**) of Ni_{5324} ANPs with heating rate of 10^6 K/s at T = 300 K.

The results from Figure 1 show that the shape of the Ni ANPs was spherical, and they were distributed quite uniformly (Figure 1a). The average coordination number (CN) was 13, and the average coordination number density (CNm) was 34.9% (Figure 1b). The link length (r) and the height of the RDF (g(r)) were determined to be 2.55 Å and 3.69 (Figure 1c), respectively. The particle size (D) was 5.023 nm, and the binding energy (E) was −0.684 eV. The obtained r value (2.55 Å) was in full agreement with the r value reported in previous studies (2.52 Å) [50]. Crystalline Ni was reported to have an r value of 2.45 Å [17,40] and 2.43 Å [49], implying that amorphous Ni always has a link length greater than the link length of crystalline Ni. This is a new finding for experimentalists doing research as well as those conducting research on the influencing factors in the following sections.

3.2. Factors Affecting the Structural Characteristic Quantities

3.2.1. Influence of the Heating Rate

The influence of the HR on the ANPs of Ni_{5324} is demonstrated in Figure 2, and the obtained results are summarized in Table 2.

The obtained results revealed the shape of the ANPs of Ni_{5324} at the HR of 5×10^5 K/s to be spherical (Figure 2a1) with D = 5.022 nm and E = −0.695 eV (Table 2). The CN was 13, and the CN_m was 33.82% (Figure 2b1). In addition, r was 2.55 Å, and g(r) was 3.69 (Figure 2c1). As clearly seen in Figure 2, raising the HR from 5×10^5 to 10^8 K/s caused a change in the shape of the ANPs of Ni_{5324} (Figure 2a1–a6). The CN was 13 and remained constant. However, the CN_m changed from 33.82 to 35.6% with the HR (Figure 2b1–b6). The r was r = 2.55 Å. However, the g(r) changed from 3.69 to 5.20 (Figure 2c1–c6). The D value increased from D = 5.022 to 16.04 nm, and the density of the atoms decreased with the increasing HR. When the HR increased from 5×10^5 to 5×10^7 K/s, the value of E increased from E = −0.695 eV to E = −0.615 eV. Finally, at 10^8 K/s, a sharp increase up to D = 16.04 nm and E = 169.119 eV (more than two orders of magnitude) was recorded (Table 2). The reason is that when the heating rate increased, the transition of the material's state accelerated (to the heating speed of 10^8 K/s). The transition of the material's state does not change in time, leading the structure break (this is also the threshold of the structural phase transition) and causing the atoms to fly out and appear empty in the materials.

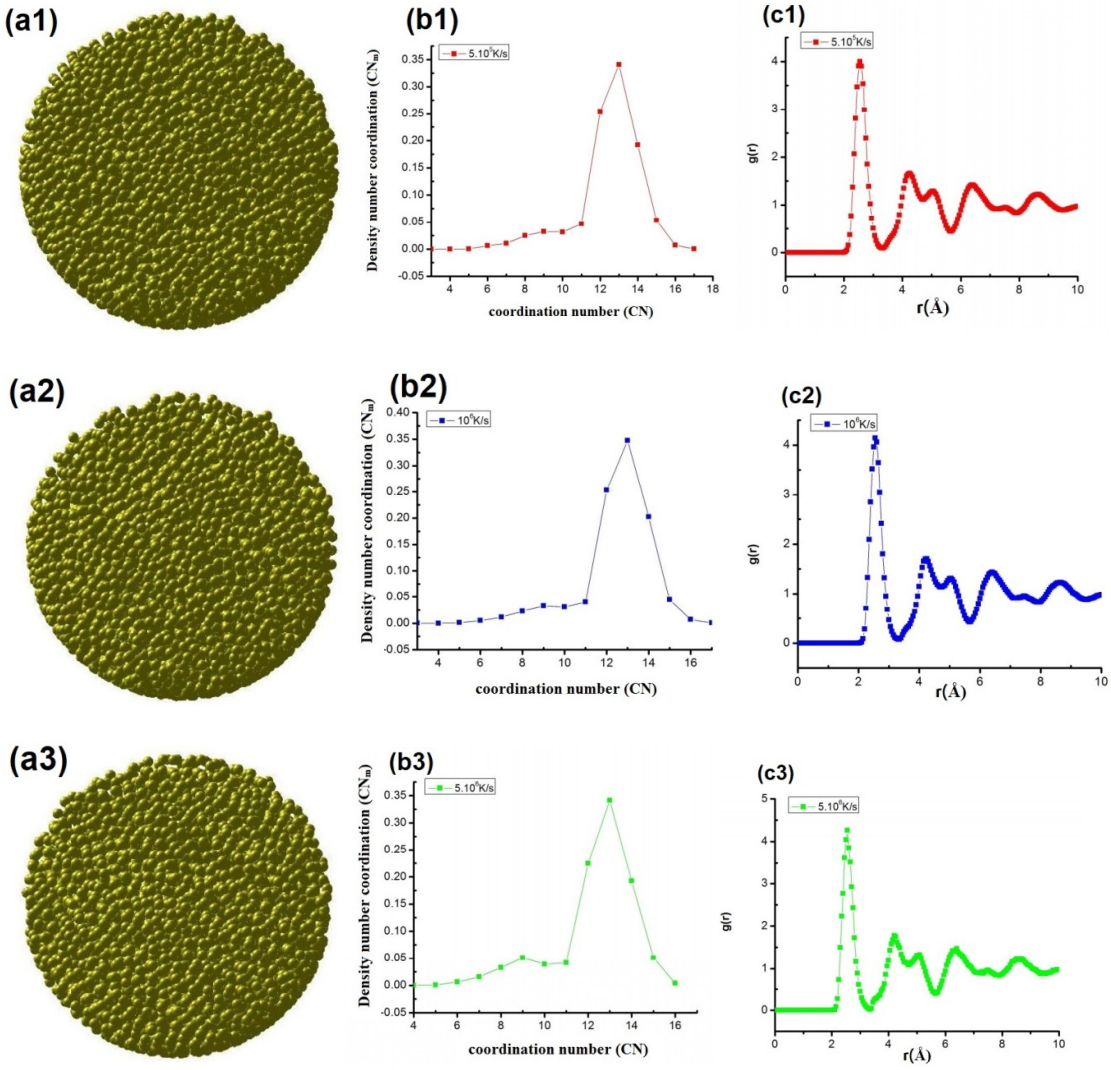

Figure 2. *Cont.*

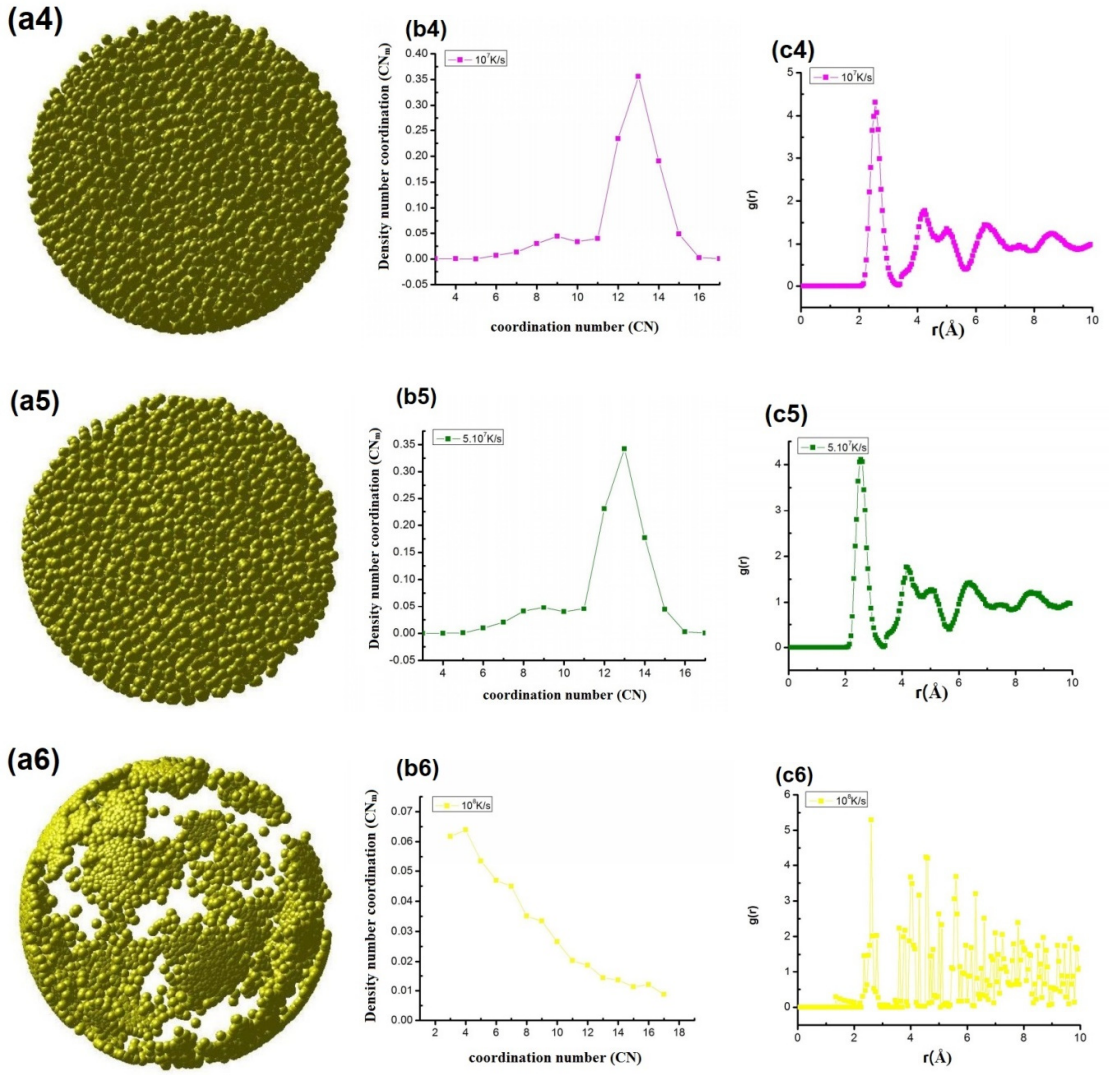

Figure 2. The shape (**a1**–**a6**), CNs (**b1**–**b6**), and RDF (**c1**–**c6**) of ANPs of Ni_{5324} with different HRs.

Table 2. D and E values for ANPs of Ni_{5324} with different HRs.

HR (K/s)	D (nm)	E (eV)	HR (K/s)	D (nm)	E (eV)
$\mathbf{5 \times 10^5}$	5.022	−0.695	$\mathbf{10^7}$	5.024	−0.659
$\mathbf{10^6}$	5.023	−0.684	$\mathbf{5 \times 10^7}$	5.024	−0.615
$\mathbf{5 \times 10^6}$	5.023	−0.673	$\mathbf{10^8}$	16.04	169.119

3.2.2. Effect of N

The influence of N on the ANPs of Ni_{2048} is demonstrated in Figure 3.

The obtained results indicated that the shape of the ANPs of Ni_{2048} was spherical and the atoms were uniformly distributed (Figure 3a). Here, the r was 2.55 Å, g(r) was 4.65; CN was 13, and CN_m was 28.13%. An increment in the N from 2048 atoms to 8788 atoms gave rise to a gradual increase in the D from 3.74 to 5.91 nm and a gradual decrease in the E from −0.657 to −0.710 eV. The r was 2.55 Å, which was consistent with the value of the ANPs of Ni obtained by the MDS method (2.52 Å) [50]. The results also revealed that the r value of the ANPs was always higher than that of the bulk material determined by the experimental method (2.43 Å) [49], and it led to a crystallization of Ni material determined by the MDS method (2.45 Å) [40]. This is because the E of the system is smaller in the crystalline or bulk material compared to the amorphous state, such that a decrease in the E

of the system causes a decrement in the bonding length. In addition, the g(r) decreased from 4.65 to 3.97, 3.83, 3.71, 3.59, and 3.70 (Figure 3b), and the CN_m decreased from 28.13 to 27.44% (Figure 3c) with increasing N values.

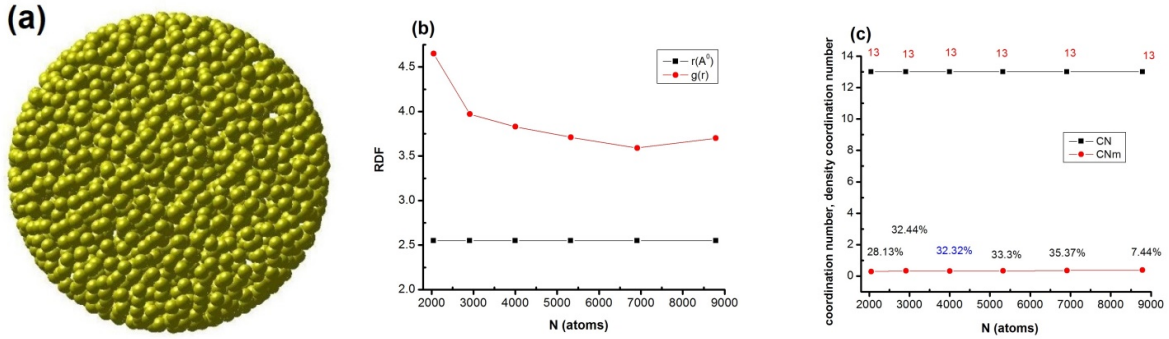

Figure 3. The shape (**a**), RDF (**b**), and CN (**c**) of the ANPs of Ni_{2048} with respect to the N.

This confirms that an increment in the N not only leads to an enhancement in the density of atoms but also the major effect of the D on the structure of the ANPs of Ni. Furthermore, the g(r) reached its maximum point (4.65) when D was 3.74 nm and its minimum point (3.59) when D was 5.42 nm. In addition, as clearly shown in Figure 4, the D increased linearly, while the E decreased linearly with increasing N values.

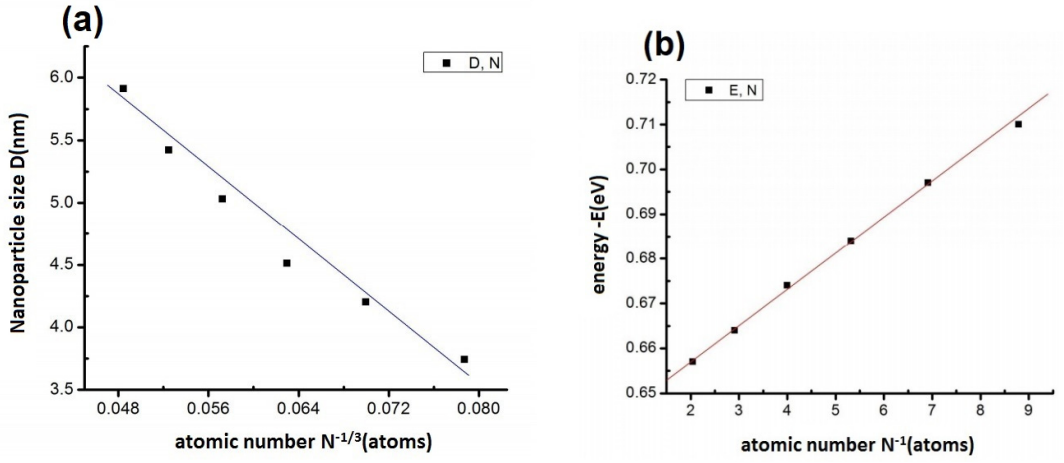

Figure 4. The correlation between the D and the N (**a**), and the correlation between the E and the N (**b**) of amorphous Ni materials with different number of atoms.

The correlations between the D and the N and between the E and the N were obtained using the equations of size where $D = 9.117 - 69.993 \cdot N^{-1/3}$ (Figure 4a) and the energy of the Ni nanoparticle is $E = 0.748 + 240 \cdot N^{-1}$ (Figure 4b), respectively, revealing that the size, D, is proportional with $N^{-1/3}$ and the energy, E, of the Ni nanoparticle is proportional with N^{-1}, respectively, as also reported in former studies [38–47].

To study the factors affecting the structure of amorphous Ni nanomaterials, we chose Ni_{5324} amorphous nanomaterials with D = 5.023 nm and E = −0.684 eV for the following steps.

3.2.3. Effect of Temperature

Figure 5 shows the impact of T on the structural features of the ANPs of Ni_{5324}.

The findings showed that the shape of the ANPs of Ni_{5324} was spherical. D = 5.023 nm and E = −0.684 eV at T = 300 K. The atoms were uniformly distributed (Figure 5a). The r of RDF was 2.55 Å, the g(r) was 3.71, the CN was 13, and the CN_m was 33.3% at T = 300 K. D and r had constant values of 5.023 nm and 2.55 Å, respectively. The E value increased gradually from E = −0.684 to E = −0.361 eV, but the g(r) value decreased gradually from

3.71 to 2.66 with the increase in T (Figure 5b). As clearly seen in Figure 5c, the CN was 13 in the range between 300 and 900 K, while it was 12 at 1100 K. The CN_m decreased from 33.3% to 29.2% with the increase in T (Figure 5c). This proved that increasing T causes a decrement in the density of atoms.

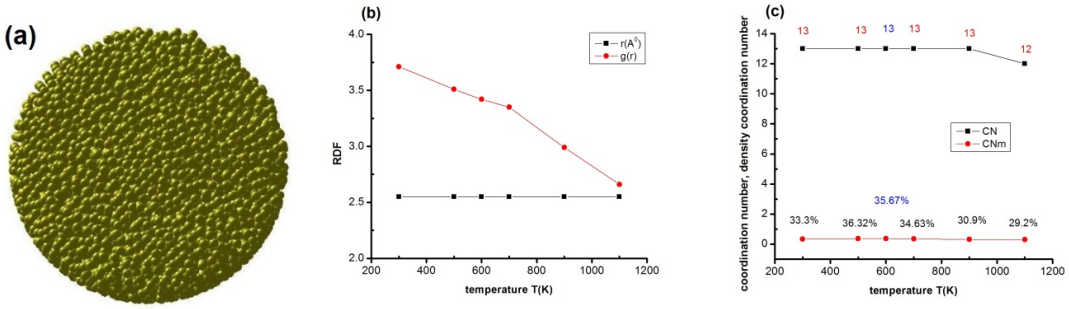

Figure 5. The shape (**a**), RDF (**b**), and CN (**c**) of the ANPs of Ni_{5324} with respect to T.

To determine the T_g value of the ANPs of Ni_{5324}, the dependence of the E on the T was examined (Figure 6).

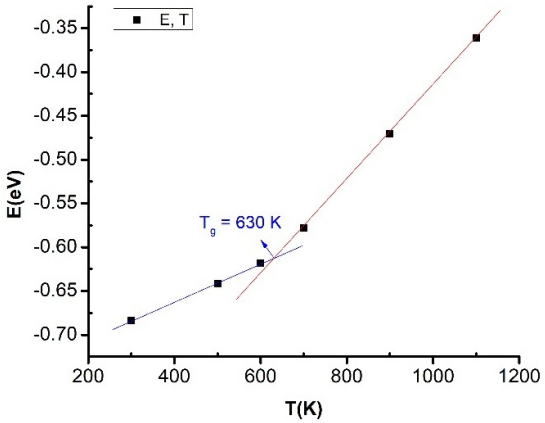

Figure 6. The T_g of the ANPs of Ni_{5324}.

As distinctly noticed in Figure 6, the E-T graph consists of two regions. It can be seen that, in both regions, there is a linear increase in the E value with increasing T. In the first region, represented by the blue line (300 K < T < 600 K), there is a weak increase in the E value with increasing T. However, in the second region, represented by the red line (T > 700 K), there is a strong increase in the E with increasing T. The red and blue lines intersect each other at T = 630 K, corresponding to E = −0.614 eV. This confirms that the T_g is 630 K, which is consistent with the T_g values reported in previous experimental and simulation studies, where T_g = 631 K [17,27,28]. The results also show that the T_g of the ANPs of Ni (630 K) revealed in this study is smaller than that of Ni NPs in the crystalline state (800 K) [45], indicating that the structure has a significant effect on the T_g of Ni NPs.

4. Conclusions

The effects of factors such as HR, N, and T on Ni ANPs were studied using the MDS method with the Pak–Doyama pair interaction potential field (PD). The investigated factors considerably affected the structural features of the ANPs of Ni. The correlations between D and E and N were determined to be $D \sim N^{-1/3}$ and $E \sim N^{-1}$. The T_g value of the ANPs of Ni, obtained from the E-T graph, was estimated to be 630 K.

The results are consistent with the T_g values reported in previous experimental and simulation studies, where T_g = 631 K. This T_g value, obtained for the ANPs of Ni (630 K), is lower than that reported for crystalline Ni NPs (800 K), revealing that the structure is one

of the key factors for the T_g. The E was proportional to N^{-1}, and the Ni-Ni link length was found to be r = 2.55 Å. This r value, obtained for the ANPs of Ni (2.55 Å), was higher than both r value of experimentally obtained bulk Ni (2.43 Å) and the r value of crystallized Ni material derived using the MDS method (2.45 Å). Concerning the role of the HR on the ANPs of Ni, it was revealed that the increase in the HR from 5×10^5 to 1×10^8 K/s induced not only a change in the shape of the Ni ANPs but also an enhancement in the D and a decrement in the density of atoms. The obtained results are expected to contribute to future empirical studies.

Author Contributions: T.T.Q.: Conceptualization and Writing—original draft. D.N.T.: Conceptualization, Methodology, Conceptualization, Investigation, Validation, Writing—original draft, Writing—review and editing, and Project administration. V.C.L.: Writing—original draft and Formal analysis. U.S.: Writing—original draft and Formal analysis. Ş.Ţ.: Writing—original draft and Writing—review and editing. All authors have read and agreed to the published version of the manuscript.

Funding: This research received no external funding.

Data Availability Statement: The data that support the findings of this study are available from the corresponding author upon reasonable request.

Conflicts of Interest: The authors declare no conflict of interest.

References

1. Rostovshchikova, T.N.; Shilina, M.I.; Golubina, E.V.; Lokteva, E.S.; Krotova, I.N.; Nikolaev, S.A.; Maslakov, K.I.; Yavsin, D.A. Adsorption and oxidation of carbon monoxide on Au and Ni nanoparticles deposited on Al_2O_3 by laser electrodispersion. *Russ. Chem. Bull.* **2015**, *64*, 812–818. [CrossRef]
2. Chandra, S.; Kumar, A.; Tomar, P.K. Synthesis of Ni nanoparticles and their characterizations. *J. Saudi Chem. Soc.* **2014**, *18*, 437–442. [CrossRef]
3. Khan, I.; Saeed, K.; Khan, I. Nanoparticles: Properties, applications and toxicities. *Arab. J. Chem.* **2019**, *12*, 908–931. [CrossRef]
4. Ali, A.; Shah, T.; Ullah, R.; Zhou, P.; Guo, M.; Ovais, M.; Tan, Z.; Rui, Y. Review on recent progress in magnetic nanoparticles: Synthesis, characterization, and diverse applications. *Front. Chem.* **2021**, *9*, 629054. [CrossRef]
5. Gatin, A.K.; Grishin, M.V.; Gurevich, S.A.; Dokhlikova, N.V.; Kirsankin, A.A.; Kozhevin, V.M.; Lokteva, E.S.; Rostovshchikova, T.N.; Sarvadii, S.Y.; Shub, B.R.; et al. Interaction of amorphous and crystalline nickel nanoparticles with hydrogen. *Russ. Chem. Bull.* **2015**, *64*, 2337–2343. [CrossRef]
6. Goryaeva, A.M.; Fusco, C.; Bugnet, M.; Amodeo, J. Influence of an amorphous surface layer on the mechanical properties of metallic nanoparticles under c ompression. *Phys. Rev. Mater.* **2019**, *3*, 033606. [CrossRef]
7. Huang, C.; Chen, X.; Xue, Z.; Wang, T. Effect of structure: A new insight into nanoparticle assemblies from inanimate to animate. *Sci. Adv.* **2020**, *6*, eaba1321. [CrossRef]
8. Jiang, W.; Guan, H.Y.; Wang, Z.; Guo, A.B. Nanoparticle with a ferrimagnetic interlayer coupling in the presence of single ion anisotropis. *Phys. B Condens. Matter* **2012**, *407*, 378–383. [CrossRef]
9. Yüksel, Y.; Aydıner, E.; Polat, H. Thermal and magnetic properties of a ferrimagnetic nanoparticle with spin-3/2 core and spin-1 shell structure. *J. Magn. Magn. Mater.* **2011**, *323*, 3168–3175. [CrossRef]
10. Ţălu, Ş.; Bramowicz, M.; Kulesza, S.; Dalouji, V.; Solaymani, S.; Valedbagi, S. Fractal features of carbon–nickel composite thin flms. *Microsc. Res. Tech.* **2016**, *79*, 1208–1213. [CrossRef]
11. Ţălu, Ş.; Bramowicz, M.; Kulesza, S.; Dalouji, V.; Ilkhani, M.; Ghaderi, A.; Solaymani, S. Infuence of annealing process on surface micromorphology of carbon–nickel composite thin flms. *Opt. Quantum Electron.* **2017**, *49*, 204. [CrossRef]
12. Hoang, V.V.; Ganguli, D. Amorphous nanoparticles—Experiments and computer simulations. *Phys. Rep.* **2012**, *518*, 81–140. [CrossRef]
13. Amodeo, J.; Lizoul, K. Mechanical properties and dislocation nucleation in nanocrystals with blunt edges. *Mater. Des.* **2017**, *135*, 223–231. [CrossRef]
14. Han, W.Z.; Huang, L.; Ogata, S.; Kimizuka, H.; Yang, Z.C.; Weinberger, C.; Li, Q.J.; Liu, B.Y.; Zhang, X.X.; Li, J.; et al. From "smaller is stronger" to "size-independent strength plateau": Towards measuring the ideal strength of iron. *Adv. Mater.* **2015**, *27*, 3385–3390. [CrossRef]
15. Huu, K.P.; Thuy, T.G.T.; Khac, H.P. The study of separation of crystal Fe and morphology for FeB nanoparticle: Molecular dynamics simulation. *AIP Adv.* **2017**, *7*, 045301. [CrossRef]
16. Trady, S.; Hasnaoui, A.; Mazroui, M.; Saadouni, K. Local atomic structures of single-component metallic glasses. *Eur. Phys. J. B* **2016**, *89*, 223. [CrossRef]
17. Minh, H.D.T.; Coman, G.; Quang, H.N.; Dung, N.T. Influence of heating rate, temperature, pressure on the structure, and phase transition of amorphous Ni material: A molecular dynamics study. *Heliyon* **2020**, *6*, e05548. [CrossRef]

18. Ţălu, Ş.; Bramowicz, M.; Kulesza, S.; Ghaderi, A.; Dalouji, V.; Solaymani, S.; Fathikenari, M.; Ghoranneviss, M. Fractal features and surface micromorphology of diamond nanocrystals. *J. Microsc.* **2016**, *264*, 143–152. [CrossRef]
19. Mahdavi, S. Nano-TiO_2 modifed with natural and chemical compounds as efcient adsorbents for the removal of Cd^{+2}, Cu^{+2}, and Ni^{+2} from water. *Clean Technol. Environ. Policy* **2016**, *18*, 81–94. [CrossRef]
20. Dalouji, V.; Solaymani, S.; Rezaee, S.; Mehrparvar, D. Nonmetal-metal transition in carbon films embed-ded by Ni nanoparticles: The temperature coefcient of resistivity (TCR), Raman spectra and surface morphology. *Optik* **2018**, *156*, 338–345. [CrossRef]
21. Yurino, T.; Ueda, Y.; Shimizu, Y.; Tanaka, S.; Nishiyama, H.; Tsurugi, H.; Sato, K.; Mashima, K. Salt-Free Reduction of Nonprecious Transition—Metal Compounds: Generation of Amorphous Ni Nanoparticles for Catalytic C–C Bond Formation. *Angew. Chem. Int. Ed.* **2015**, *54*, 14437–14441. [CrossRef] [PubMed]
22. Ruan, Y.; Wang, C.; Jiang, J. Nanostructured Ni compounds as electrode materials towards high-performance electrochemical capacitors. *J. Mater. Chem. A* **2016**, *4*, 14509–14538. [CrossRef]
23. Xu, R.; Xie, T.; Zhao, Y.; Li, Y. Quasi-homogeneous catalytic hydrogenation over monodisperse nickel and cobalt nanoparticles. *Nanotechnology* **2007**, *18*, 055602. [CrossRef]
24. Wang, D.P.; Sun, D.B.; Yu, H.Y.; Qiu, Z.G.; Meng, H.M. Preparation of one-dimensional nickel nanowires by self-assembly process. *Mater. Chem. Phys.* **2009**, *113*, 227–232. [CrossRef]
25. Trady, S.; Mazroui, M.; Hasnaoui, A.; Saadouni, K. Molecular dynamics study of atomic-level structure in monatomic metallic glass. *J. Non-Cryst. Solids* **2016**, *443*, 136–142. [CrossRef]
26. Fedorchenko, A.I. On the glass transition of the one-component metallic melts. *J. Cryst. Growth.* **2017**, *475*, 362–367. [CrossRef]
27. He, X.; Shi, H. Size and shape effects on magnetic properties of Amorphous Ni nanoparticles. *Particuology* **2012**, *10*, 497–502. [CrossRef]
28. Sun, C.Q.; Zhong, W.H.; Li, S.; Tay, B.K.; Bai, H.L.; Jiang, E.Y. Coordination imperfection suppressed phase stability of ferromagnetic, ferroelectric, and superconductive nanosolids. *J. Phys. Chem. B* **2004**, *108*, 1080–1084. [CrossRef]
29. Asareh, N.; Dalouji, V.; Solaymani, S.; Rezaee, S. Relation between carriers hopping rate and structural constants in amorphous carbon nickel flms with diferent nickel nanoparticles distributions. *Opt. Quantum Electron.* **2019**, *51*, 373. [CrossRef]
30. Peng, Y.; Chen, Q.; Xie, J.; Lan, W. Communication-Facile Synthesis of Amorphous Nickel Boride Nanoparticles for Highly Sensitive Non-Enzyme Glucose Detection. *J. Electrochem. Soc.* **2019**, *166*, B521–B523. [CrossRef]
31. Cargnello, M. Colloidal Nanocrystals as Building Blocks for Well-Defined Heterogeneous Catalysts. *Chem. Mater.* **2019**, *31*, 576–596. [CrossRef]
32. Vogt, C.; Groeneveld, E.; Kamsma, G.; Nachtegaal, M.; Lu, L.; Kiely, C.J.; Berben, P.H.; Meirer, F.; Weckhuysen, B.M. Unravelling structure sensitivity in CO_2 hydrogenation over nickel. *Nat. Catal.* **2018**, *1*, 127–134. [CrossRef]
33. Gao, J.; Liu, Q.; Gu, F.; Liu, B.; Zhong, Z.; Su, F. Recent advances in methanation catalysts for the production of synthetic natural gas. *RSC Adv.* **2015**, *5*, 22759–22776. [CrossRef]
34. Zacharaki, E.; Beato, P.; Tiruvalam, R.R.; Andersson, K.J.; Fjellvåg, H.; Sjåstad, A.O. From Colloidal Monodisperse Nickel Nanoparticles to Well-Defined Ni/Al_2O_3 Model Catalysts. *Langmuir* **2017**, *33*, 9836–9843. [CrossRef]
35. Li, Y.; Wen, J.; Ali, A.M.; Duan, M.; Zhu, W.; Zhang, H.; Chen, C.; Li, Y. Size structure–catalytic performance correlation of supported Ni/MCF-17 catalysts for CO_x-free hydrogen production. *Chem. Commun.* **2018**, *54*, 6364–6367. [CrossRef]
36. Laprune, D.; Tuel, A.; Farrusseng, D.; Meunier, F.C. Highly dispersed nickel particles encapsulated in multi-hollow silicalite-1 single crystal nanoboxes: Effects of siliceous deposits and phosphorous species on the catalytic performances. *ChemCatChem* **2017**, *9*, 2297–2307. [CrossRef]
37. Goodarzi, F.; Kang, L.; Wang, F.R.; Joensen, F.; Kegnaes, S.; Mielby, J. Methanation of Carbon Dioxide over Zeolite-Encapsulated Nickel Nanoparticles. *ChemCatChem* **2018**, *10*, 1566–1570. [CrossRef]
38. Wen, Y.H.; Zhu, Z.Z.; Zhu, R.; Shao, G.F. Size effects on the melting of nickel nanowires: A molecular dynamics study. *Phys. E* **2004**, *25*, 47–54. [CrossRef]
39. Kien, P.H.; Lan, M.T.; Dung, N.T.; Hung, P.K. Annealing study of amorphous bulk and nanoparticle iron using molecular dynamics simulation. *Int. J. Mod. Phys. B* **2014**, *28*, 1450155. [CrossRef]
40. Nguyen, T.N.; Nguyen, C.C.; Tran, V.H. Molecular dynamics study of microscopic structures, phase transitions and dynamic crystallization in Amorphous Ni nanoparticles. *RSC Adv.* **2017**, *7*, 25406–25413. [CrossRef]
41. Qi, Y.; Çağin, T.; Johnson, W.L.; Goddard, W.A., III. Melting and crystallization in Ni nanoclusters: The mesoscale regime. *J. Chem. Phys.* **2001**, *115*, 385–394. [CrossRef]
42. Andriotis, A.N.; Fthenakis, Z.G.; Menon, M. Correlated variation of melting and Curie temperatures of nickel clusters. *Phys. Rev. B* **2007**, *75*, 073413. [CrossRef]
43. Dung, N.T. Influence of impurity concentration, atomic number, temperature and tempering time on microstructure and phase transformation of $Ni_{1-x}Fe_x$ (x = 0.1, 0.3, 0.5) nanoparticles. *Mod. Phys. Lett. B* **2018**, *32*, 1850204. [CrossRef]
44. Tuan, T.Q.; Dung, N.T. Effect of heating rate, impurity concentration of Cu, atomic number, temperatures, time annealing temperature on the structure, crystallization temperature and crystallization process of $Ni_{1-x}Cu_x$ bulk; x = 0.1, 0.3, 0.5, 0.7. *Int. J. Mod. Phys. B* **2018**, *32*, 1830009. [CrossRef]
45. Zhang, Y.; Wang, L.; Wang, W. Thermodynamic, dynamic and structural relaxation in supercooled liquid and glassy Ni below the critical temperature. *J. Phys. Cond. Matter.* **2007**, *19*, 196106. [CrossRef]

46. Kelchner, C.L.; Plimpton, S.J.; Hamilton, J.C. Dislocation nucleation and defect structure during surface indentation. *Phys. Rev. B* **1998**, *58*, 11085–11088. [CrossRef]
47. Tian, C.S.; Qian, D.; Wu, D.; He, R.H.; Wu, Y.Z.; Tang, W.X.; Yin, L.F.; Shi, Y.S.; Dong, G.S.; Jin, X.F.; et al. Body-Centered-Cubic Ni and Its Magnetic Properties. *Phys. Rev. Lett.* **2005**, *94*, 137210. [CrossRef]
48. Lu, H.M.; Li, P.Y.; Cao, Z.H.; Meng, X.K. Size, shape, and dimensionality-dependent melting temperatures of nanocrystals. *J. Phys. Chem. C* **2009**, *113*, 7598–7602. [CrossRef]
49. Ichikawa, T. Electron diffraction study of the local atomic arrangement in amorphous Iron and Nickel films. *Phys. Status Solidi A* **1973**, *19*, 707–716. [CrossRef]
50. Kien, P.H. Study of structural transition of nickel metal under temperature. *Ph. Transit.* **2016**, *90*, 732–741.
51. Dung, N.T.; Van, C.L. Effects of number of atoms, shell thickness, and temperature on the structure of Fe nanoparticles amorphous by molecular dynamics method. *Adv. Civ. Eng.* **2021**, *2021*, 9976633.
52. Quoc, T.T.; Trong, D.N. Molecular dynamics factors affecting on the structure, phase transition of Al bulk. *Phys. B Condens. Matter* **2019**, *570*, 116–121. [CrossRef]
53. Trong, D.N.; Tri, P.N. Understanding the heterogeneous kinetics of Al nanoparticles by simulations method. *J. Mol. Struct.* **2020**, *1218*, 128498. [CrossRef]
54. Dung, N.T.; Cuong, N.C.; Van, D.Q.; Tuan, T.Q. Study the effects of factors on the structure and phase transition of bulk Ag by molecular dynamics method. *Int. J. Comput. Mater. Sci. Eng.* **2020**, *09*, 2050016.
55. Trong, D.N.; Long, V.C.; Ţălu, Ş. Molecular dynamics simulation of bulk Cu material pseudo-crystallization under various factors. *Appl. Sci.* **2022**, *12*, 4437. [CrossRef]
56. Trong, D.N. Z-AXIS deformation method to investigate the influence of system size, structure phase transition on mechanical properties of bulk nickel. *Mater. Chem. Phys.* **2020**, *252*, 123275. [CrossRef]
57. Tsuzuki, H.; Branicio, P.S.; Rino, J.P. Structural characterization of deformed crystals by analysis of common atomic neighborhood. *Comput. Phys.Commun.* **2007**, *177*, 518–523. [CrossRef]
58. Lu, J.; Szpunar, J.A. Applications of the embedded-atom method to glass formation and crystallization of liquid and glass transition-metal nickel. *Philos. Mag. A* **1997**, *75*, 1057–1066. [CrossRef]
59. Yamamoto, R.; Mihara, T.; Taira, K.; Doyama, M. Amorphous structures of iron obtained by quenching of the liquid state. *Phys. Lett. A* **1979**, *70*, 41–43. [CrossRef]
60. Nosé, S. A unified formulation of the constant temperature molecular dynamics methods. *J. Chem. Phys.* **1984**, *81*, 511–519. [CrossRef]
61. Hoover, W.G. Canonical dynamics: Equilibrium phase-space distributions. *Phys. Rev. A* **1985**, *31*, 1695–1697. [CrossRef] [PubMed]
62. Lacks, D.J. First-order amorphous-amorphous transformation in silica. *Phys. Rev. Lett.* **2000**, *84*, 4529–4532. [CrossRef] [PubMed]
63. Guitierrez, G.; Johansson, B. Molecular dynamics study of structural properties of amorphous Al_2O_3. *Phys. Rev. B* **2002**, *65*, 104202–104210. [CrossRef]
64. Hoang, V.V. Glass of monatomic Lennard-Jones system at nanoscale. *Phys. B Condens. Matter* **2010**, *405*, 1908–1914. [CrossRef]
65. Hoang, V.V.; Odagaki, T.; Engel, M. Cooling rate effects on structure and thermodynamics of amorphous nanoparticles. *Appl. Surf. Sci.* **2008**, *254*, 7531–7534. [CrossRef]
66. Li, J. AtomEye: An efficient atomistic configuration viewer. *Model. Simul. Mater. Sci. Eng.* **2003**, *11*, 173. [CrossRef]
67. Ackland, G.J.; Jones, A.P. Applications of local crystal structure measures in experiment and simulation. *Phys. Rev. B* **2006**, *73*, 054104. [CrossRef]
68. Steinhardt, P.J.; Nelson, D.R.; Ronchetti, M. Bond-Orientational Order in Liquids and Glasses. *Phys. Rev. B* **1983**, *28*, 784–805. [CrossRef]
69. Francesco, T.; Arrigo, C. Multi-technique approach to unravel the (dis)order in amorphous materials. *ACS Omega* **2022**, *7*, 23255–23264.